Journal of Nanoparticle Research **2:** 333–344, 2000.

Invited paper

Forces that drive nanoscale self-assembly on solid surfaces

Z. Suo and W. Lu
Department of Mechanical and Aerospace Engineering, Princeton Materials Institute, Princeton University, Suite D404, Eng. Quadrangle, Princeton, NJ 08544, USA (Tel.: 609-258-0250; Fax: 609-258-5877; E-mail: suo@princeton.edu)

Received 17 August 2000; accepted in revised form 11 October 2000

Key words: nanostructure, epitaxial film, self-assembly, surface stress, phase separation, nanoparticles

Abstract

Experimental evidence has accumulated in the recent decade that nanoscale patterns can self-assemble on solid surfaces. A two-component monolayer grown on a solid surface may separate into distinct phases. Sometimes the phases select sizes about 10 nm, and order into an array of stripes or disks. This paper reviews a model that accounts for these behaviors. Attention is focused on thermodynamic forces that drive the self-assembly. A double-welled, composition-dependent free energy drives phase separation. The phase boundary energy drives phase coarsening. The concentration-dependent surface stress drives phase refining. It is the competition between the coarsening and the refining that leads to size selection and spatial ordering. These thermodynamic forces are embodied in a nonlinear diffusion equation. Numerical simulations reveal rich dynamics of the pattern formation process. It is relatively fast for the phases to separate and select a uniform size, but exceedingly slow to order over a long distance, unless the symmetry is suitably broken.

Introduction

In the solid state, atoms can diffuse from one site to another, giving rise to conspicuous changes over time. In some circumstances, atoms may self-assemble into a periodic structure, such as an array of stripes or dots. The feature size may be of nanoscale, small compared to bulk structures, but large compared to individual atoms. In this intermediate size range, new phenomena appear. Why do atoms self-assemble? What sets the feature size? The answers differ for different material systems. A unifying concept, however, can be identified. For many reasons the free energy of a material system depends on its configuration (e.g., the composition of the phases and their spatial arrangement). When the configuration changes, the free energy also changes. This defines thermodynamic forces that drive the configuration change. The change is effected by mass transport processes, such as diffusion. To assemble a nanostructure, some of the forces must act over the scale comparable to the feature size, and are therefore much longer ranging than atomic bond length. The long-range forces have various physical origins, including elasticity, electrostatics, magnetostatics, photon dispersion, and electron confinement (Ng and Vanderbilt, 1995; Murray et al., 2000; Suo, 2000). They lead to self-assembly in diverse material systems (e.g., Chen & Khachaturyan, 1993; Seul & Andelman, 1995; BaIl, 1999; Böhringer, 1999).

To discuss configurational forces in action, this paper focuses on a particular phenomenon: nanoscale phase patterns on solid surfaces. Studies of nanoscopic activities on solid surfaces have surged after the invention of the Scanning Tunneling Microscopy (STM). Figure 1a is a schematic of an observed pattern. Kern et al. (1991) exposed a copper surface to gaseous oxygen of low

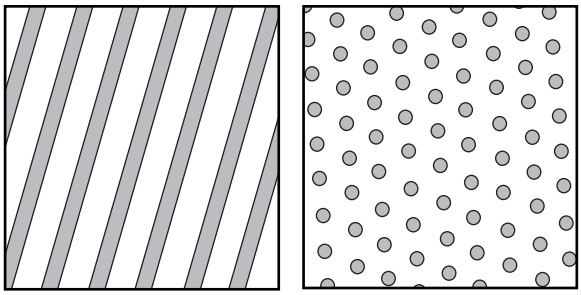

(a) (b)

Figure 1. Schematics of experimentally observed nanoscale patterns on solid surfaces. (a) Alternating stripes. (b) A lattice of dots.

pressure. An atomic thick superficial oxide formed, covering a fraction of the copper surface, and ordering into stripes that alternate with bare copper stripes. The width of the stripes was on the order of 10 nm. Another example is illustrated in Figure 1b. Pohl et al. (1999) deposited a monolayer of silver on a ruthenium surface, and then exposed the silver-covered ruthenium to sulfur. The epilayer became a composite of sulfur disks in a continuous silver matrix. The sulfur disks were of diameter about 3.4 nm, and formed a triangular lattice. The observations common to both systems are phase separation, size selection, and spatial ordering within monolayers on solid surfaces. Similar observations have been made in other material systems (e.g., Parker et al., 1997; Brune et al., 1998). On the other hand, not all two-phase monolayers self-assemble into periodic structures (e.g., Röder et al., 1993; Clark & Friend, 1999).

These intriguing experimental observations have stimulated theoretical studies. Vanderbilt (1997) has reviewed a model based on surface stresses and phase boundary energy. The model shows that superlattices of stripes and dots minimize the net free energy. Similar energetic forces have been incorporated in a phase field model, which we have used to study the dynamic process of self-assembly (Lu & Suo, 1999, 2001; Suo & Lu, 2000a,b). Our study shows that it is relatively fast for the phases to separate and select a uniform size, but exceedingly slow to order over a long distance, unless suitable symmetry breaking takes place. The object of this paper is to review the physical ingredients to account for the experimental observations, their mathematical representations, and the results of numerical simulation. To limit the scope of this review, we will follow mainly the development of the phase field model.

Phase separation, phase coarsening, and phase refining

Imagine a monolayer of two atomic species A and B grown on a substrate of atomic species S. As illustrated in Figure 2, the monolayer separates into two phases α and β. The substrate occupies the half space $x_3 < 0$, bounded by the x_1–x_2 plane. The in-plane phase size is in the order 10 nm, much larger than the atomic dimension. Consequently, we will neglect the discreteness of individual atoms. For example, the model will not recognize the height of the atomic steps on the surface. Two situations are considered. Figure 3a illustrates a cross-sectional view of the α phase covering a fraction of the substrate surface, the bare substrate surface itself being the second phase. In Figure 3b, the topmost monolayer comprises two phases α and β that both differ from the substrate. The two situations are described in the same model in the following. Before delving into the mathematics of the model, we first discuss qualitatively the physical ingredients needed to account for the experimental observations.

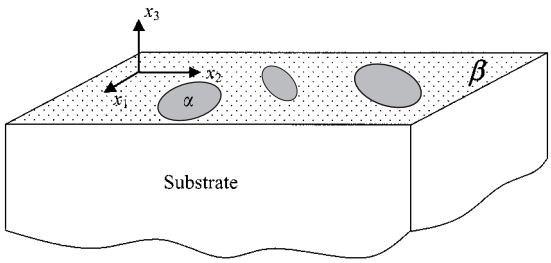

Figure 2. The geometry of the model. A two-phase monolayer on a semi-infinite substrate.

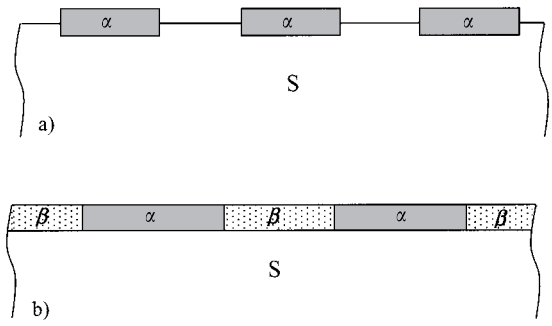

Figure 3. (a) A submonolayer of α phase on the substrate. The bare substrate is the second phase. (b) A two-phase monolayer on a substrate.

During deposition, when atoms hit the substrate, their initial positions are random. To collectively self-assemble into a nanostructure, the individual atoms must be mobile on the surface. We assume that atoms move by diffusion on the surface. To maintain a flat monolayer on the solid surface, we further assume that atoms diffuse within the topmost monolayer – that is, atoms neither diffuse into the bulk of the substrate, nor pile up into three dimensional islands. For the time being, the concentration in the monolayer is constrained to be uniform. The mixing of the two species increases entropy. The system relaxes to an equilibrium state (subject to the constraint of concentration uniformity) by accommodating the misfits among the three kinds of atoms and the free space. The misfits alter electronic states and the free energy of the system. The effect is short-ranging in that atoms in the substrate, a few monolayers beneath the epilayer, have the same energy as those in an infinite elemental crystal of S. We lump the epilayer, together with those adjacent monolayers of the substrate affected by the atomic misfit, into a single superficial object.

Consider phase separation. Let C be the concentration, i.e., the fraction of component B in the monolayer. The free energy per unit area of the superficial object is a function of the concentration, $g(C)$. When this function is non-convex, the monolayer may separate into distinct phases. The process is understood as follows, analogous to a bulk mixture. Figure 4 illustrates a double-welled function $g(C)$. A tangent line contacts the function at two concentrations, C_α and C_β. We now remove the constraint and allow the concentration in the monolayer to become nonuniform. For a monolayer with the average concentration C_{ave} between C_α and C_β, the monolayer reduces its free energy by separating into two phases of the concentrations C_α and C_β. The model with the ingredient of a double-welled function $g(C)$ accounts for phase separation; however, the model does not account for size selection or spatial ordering. The free energy of the system is the function $g(C)$ integrated over the monolayer. No length scale exists in the model: the size and the spatial arrangement of the phases do not affect the free energy.

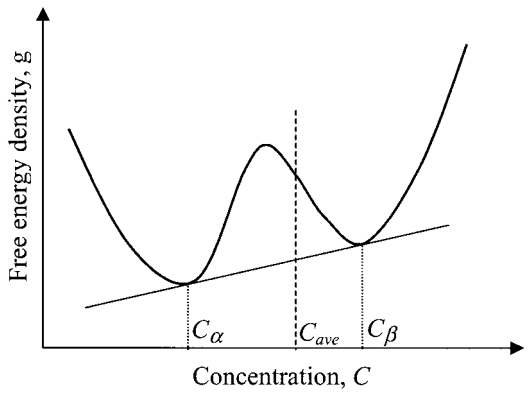

Figure 4. A double-welled function $g(C)$ causes phase separation. A tangent line contact the function at two concentrations, corresponding to two phases in equilibrium. A mixture with the average concentration between these two concentrations will separate into the two phases.

To prevent the phases from refining all the way to the atomic scale, the model needs another ingredient: phase coarsening. This is readily available from the excess free energy of the phase boundaries. Figure 5 illustrates the snapshots of a monolayer mixture at two times. Say the α phase forms disks in a continuous matrix of the β phase. The free energy increases with the total length of the phase boundary. During the process of evolution, the total area of each phase is essentially invariant. When the disks are small, the collective phase boundary is long. To reduce the free energy, atoms diffuse, so that the large disks grow larger, and small ones disappear. This model, which combines phase separation and phase coarsening, is a two dimensional analogue of the model for such bulk two-phase mixtures as oil droplets in water, or the θ phase (AI_2Cu) precipitates in aluminum (Martin et al., 1997). Time permitting, the monolayer will evolve into a single large disk of the α phase in the matrix of the β phase.

To prevent the phases from coarsening to bulk sizes, we must introduce yet another ingredient: phase refining. The superficial alloy is not really two-dimensional; rather, it couples with the substrate through elastic strains. Atoms near the surface are subject to a residual stress field, known as the surface stress (Cammarata, 1994; Ibach, 1997). A more rigorous definition of the

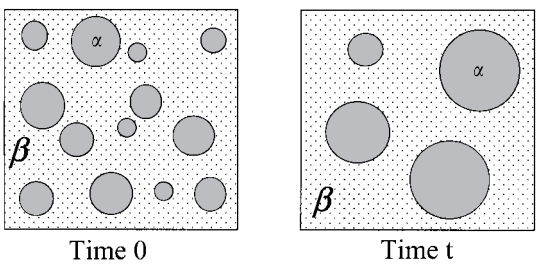

Figure 5. Snapshots of a mixture at two times. The phase boundary energy drives phases coarsening.

surface stress will be discussed later. For now, let us see how this residual stress field causes phase refining. When the monolayer is a two-phase mixture, each phase has its own surface stress. The difference in the surface stresses in the two phases induces an elastic field in the substrate, and thereby changes the free energy of the system. Figure 6 illustrates the concept. Imagine a 'cut and paste' operation. Start with a pure α phase monolayer on the substrate (Figure 6a), and a pure β phase monolayer on the substrate (Figure 6b). In both structures (a) and (b), the surface stresses are uniform, denoted as f_α and f_β. To be definite in the following discussion, say $f_\alpha > f_\beta$ and let $\Delta f = f_\alpha - f_\beta$. When the concentration is uniform in the monolayers, the semi-infinite substrates are unstrained. Cut from the structures in Figure 6a and b and paste into the two phase monolayer in Figure 6c. Maintain the residual stresses in the two phases as f_α and f_β by applying the forces Δf at the phase boundaries in the directions as shown. In state (c) the substrate is still unstrained. We then relax the structure from state (c) to state (d) by gradually releasing the applied force Δf. In the process, the α phase contracts, the β phase expands, and the substrate deforms accordingly. The release of the force Δf reduces the net elastic energy stored in the system.

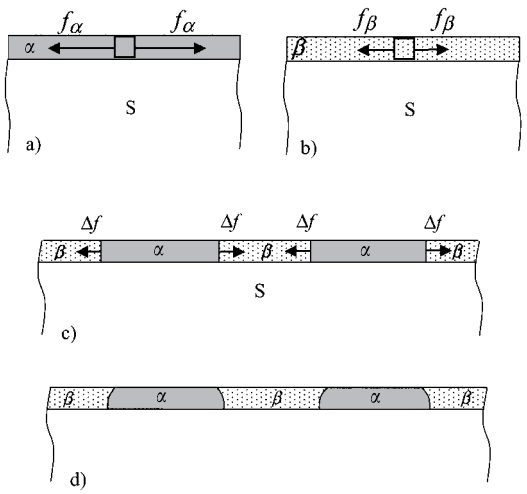

Figure 6. Nonuniform surface stress causes phase refining. (a) A uniform α phase monolayer on the substrate. The surface stress f_α is uniform, and the substrate is unstressed. (b) A uniform β phase monolayer on the substrate. The surface stress f_β is uniform, and the substrate is unstressed. (c) A two-phase monolayer on the substrate. The force Δf is applied on the phase boundaries to maintain the surface stresses f_α and f_β in the two phases, and the substrate is unstressed. (d) The applied forces Δf is relieved and the elastic energy is reduced. The α phase contracts, and the β phase expands. The substrate is now stressed.

Evidently, the more refined the phases, the more elastic energy can be reduced – that is, the concentration-dependent surface stress causes phase refining. On the other hand, as the phases refine, more phase boundaries are introduced into the monolayer, raising the total free energy. It is the competition between the coarsening due to the phase boundary energy and refining due to the nonuniform surface stress that selects a phase size. The quantitative analysis below will show that this competition gives rise to the nanoscale phase size. Furthermore, the elastic field in the substrate leads to spatial ordering of the phases in the monolayer.

Kinematics, energetics, and kinetics

It is clear from the above discussion that, to account for self-assembling phases in a monolayer, a model should contain the following ingredients: phase separation, phase coarsening, and phase refining. Each ingredient may be given alternative mathematical representations. We next summarize a model proposed by Suo and Lu (2000a). This section reviews, in turn, the kinematics, the energetics, and the kinetics of the model. The model results in a nonlinear diffusion equation of the Cahn–Hilliard type, which is summarized in the next section.

First let us specify the kinematics, namely, the means by which the configuration changes. As shown in Figure 7, the system can vary in two ways: elastic

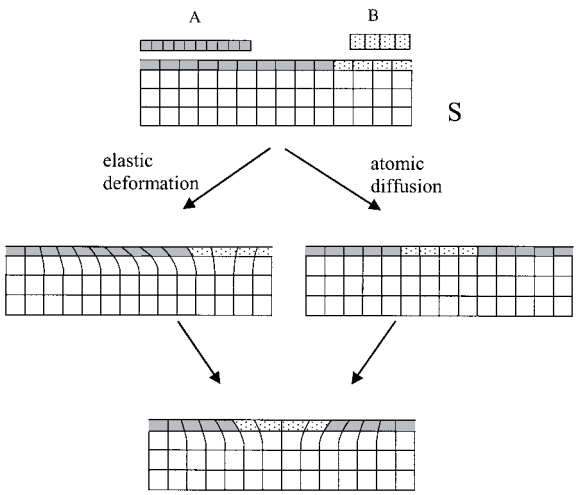

Figure 7. The configuration can vary by two means: elastic deformation and atomic diffusion.

deformation, in which atoms do not exchange positions; and atomic diffusion, in which the substrate does not deform. The two processes are concurrent in reality. Nonetheless it is convenient to consider them separately. To specify elastic deformation, we take the reference state to be an infinite, unstressed S crystal. When a semi-infinite crystal of S atoms and a monolayer of A and B atoms are assembled, the system is first constrained so that all S atoms assume the positions of the reference state. The system is then relaxed to allow deformation. Let u_i be the displacement vector of a material particle in the relaxed substrate relative to the same particle in the reference state. A Latin subscript runs from 1 to 3. The strain tensor ε_{ij} relates to the displacement gradient tensor in the usual way:

$$\varepsilon_{ij} = \tfrac{1}{2}(u_{i,j} + u_{j,i}). \tag{1}$$

The monolayer is taken to be coherent on the substrate. In the reference state, where the substrate is unstressed, the monolayer is typically under residual stress. When the substrate deforms, the monolayer deforms by the same amount as the substrate surface. Let u_α be the displacement field in the plane of the substrate surface. A Greek subscript runs from 1 to 2. The strain tensor in the surface is $\varepsilon_{\alpha\beta} = (u_{\alpha,\beta} + u_{\beta,\alpha})/2$.

We next consider atomic diffusion. Imagine a curve lying in the substrate surface. When some number of A-atoms cross the curve, to maintain a flat epilayer, an equal number of B-atoms must cross the curve in the opposite direction. Denote the unit vector lying in the surface normal to the curve by $\boldsymbol{m}$. Define a vector field $\boldsymbol{I}$ in the surface (called the mass relocation), such that $I_\alpha m_\alpha$ is the number of B-atoms across a unit length of the curve. A repeated index implies summation. Mass conservation requires that the variation in the concentration relate to the variation in the mass relocation as

$$\Lambda \delta C = -\delta I_{\alpha,\alpha}, \tag{2}$$

where Λ is the number of atomic sites per unit area. Similarly define a vector field $\boldsymbol{J}$ (called the mass flux), such that $J_\alpha m_\alpha$ is the number of B-atoms across a unit length of the curve on the surface per unit time. The relation between $\boldsymbol{I}$ and $\boldsymbol{J}$ is analogous to that between displacement and velocity. The time rate of the concentration compensates the divergence of the flux vector, namely,

$$\Lambda \partial C/\partial t = -J_{\alpha,\alpha}. \tag{3}$$

Following the qualitative description in the last section, we now specify the energetics, namely, the forces that drive the configurational changes. Let the reference state for the free energy be atoms in three unstressed, infinite, pure crystals of A-, B-, and S-atoms. When atoms are taken from this reference state to form the monolayer–substrate composite, the free energy changes due to the entropy of mixing, the misfits among the three kinds of atoms, and the presence of the free space. In addition, the misfits can induce an elastic field in the substrate. Let G be the free energy of the entire composite relative to the reference state of the three elemental crystals. The free energy consists of two parts: bulk and the surface, namely,

$$G = \int W\, dV + \int \Gamma\, dA. \tag{4}$$

The first integral extends over the volume of the entire system, W being the elastic energy per unit volume. The second integral extends over the surface area, Γ being the surface energy per unit area. Both the volume and the surface are measured in the unstressed substrate. As a convention we extend the value of the substrate elastic energy W all the way into the superficial object. Consequently, the surface energy Γ is the excess free energy in the superficial object in addition to the substrate elastic energy. The convention follows the one that defines the surface energy for a one-component solid (Cammarata, 1994).

The elastic energy per unit volume, W, takes the usual form. We assume that the substrate is isotropic, with Young's modulus E and Poisson's ratio ν. The elastic energy density function is quadratic in the strain tensor, given by

$$W = \frac{E}{2(1+\nu)}\left[\varepsilon_{ij}\varepsilon_{ij} + \frac{\nu}{1-2\nu}(\varepsilon_{kk})^2\right]. \tag{5}$$

The stresses σ_{ij} are the differential coefficients, namely,

$$\delta W = \sigma_{ij}\delta\varepsilon_{ij}. \tag{6}$$

The combination of Eqs. (5) and (6) gives Hooke's law that linearly relates the stress components to the strain components.

The surface energy per unit area, Γ, takes an unusual from. Assume that Γ is a function of the concentration C, the concentration gradient $C_{,\alpha}$ and the strains in the surface, $\varepsilon_{\alpha\beta}$. Expand the function $\Gamma(C, C_{,\alpha}, \varepsilon_{\alpha\beta})$ into the Taylor series to the leading order terms in the concentration gradient and the strains, namely,

$$\Gamma = g(C) + h(C)C_{,\beta}C_{,\beta} + f(C)\varepsilon_{\alpha\beta}, \tag{7}$$

where g, f and h are all functions of the concentration C. We have assumed isotropy in the plane of the surface; otherwise both f and h should be replaced by second rank tensors. The leading order term in the concentration gradient is quadratic because, by symmetry, the term linear in the concentration gradient does not affect the surface energy. We have neglected terms quadratic in the displacement gradient tensor, which relate to the excess in the elastic constants of the epilayer relative to the substrate. The physical content of Eq. (7) is understood term by term as follows.

When the concentration field is uniform in the epilayer, the substrate is unstrained, and the function $g(C)$ is the only remaining term in G. As discussed above, $g(C)$ is the excess energy per unit area of the superficial object. If non-convex, the function $g(C)$ drives phase separation. The function favors neither coarsening nor refining.

We assume that $h(C)$ is a positive constant, $h(C) = h_0$. Any nonuniformity in the concentration field by itself increases the free energy Γ. Consequently, the second term in Eq. (7) represents the phase boundary energy; the term drives phase coarsening. The first two terms in Eq. (7) are analogous to those in the model of bulk phase separation of Cahn and Hilliard (1958). The model represents a phase boundary by a concentration gradient field. An alternative model represents a phase boundary by a sharp discontinuity (Vanderbilt, 1997). The merits of the two kinds of models have been discussed in the literature on bulk alloys (e.g., Chen & Wang, 1996; Su & Voorhees, 1996). The phase field model does not need to track the location of the phase boundaries, and therefore readily allows topological changes in the phase pattern. For the present problem, the phase field model also circumvents elastic singularity which were present if a phase boundary were represented by a sharp discontinuity.

Now look at the last term in Eq. (7). By definition, f is the change in the surface energy associated with per unit elastic strain. Consequently, f represents the surface stress. More precisely, it is the resultant force per unit length in the superficial object. Ibach (1997) has reviewed the experimental information on the function $f(C)$. For simplicity, we assume that the surface stress is a linear function of the concentration:

$$f(C) = \psi + \phi C, \tag{8}$$

where ψ is the surface stress when the monolayer comprises pure A-atoms, and ϕ is the slope. When the concentration is nonuniform in the monolayer, the surface stress is also nonuniform, and induces an elastic field in the substrate. Such an elastic field will refine phases. It is evident that only the slope ϕ affects phase patterning. The constant surface stress ψ does not.

As discussed above, the monolayer–substrate as a thermodynamic system can vary by two means: elastic displacement variation δu_i and atomic relocation variation δI_α . A direct calculation gives the variation in the free energy:

$$\delta G = \int f \delta u_{\alpha,\alpha}\, dA + \int \sigma_{ij} \delta u_{i,j}\, dV + \int \frac{\partial}{\Lambda \partial x_\alpha} \left(\frac{\partial g}{\partial C} - 2h_0 \nabla^2 C + \phi \varepsilon_{\beta\beta} \right) \delta I_\alpha\, dA. \tag{9}$$

The first two integrals are associated with the elastic displacement variation, and the last with the atomic relocation variation. In writing Eq. (9), we have discarded integrals along lines on the surface, assuming periodical boundary conditions. The system attains thermodynamic equilibrium when $\delta G = 0$ for arbitrary variations δu_i and δI_α.

We will study states of partial equilibrium, in which the free energy variation associated with the elastic displacement variation vanishes, but that associated with atomic diffusion does not. That is, diffusion is so slow that the solid is in elastic equilibrium at all time. Consequently, the integral in Eq. (9) associated with δu_i vanishes:

$$\int f \delta u_{\alpha,\alpha}\, dA + \int \sigma_{ij} \delta u_{i,j}\, dV = 0. \tag{10}$$

This is a variational statement of an elasticity problem. In addition to the standard elasticity equations (Timoshenko & Goodier, 1970), it gives the boundary conditions:

$$\sigma_{3\alpha} = \partial f / \partial x_\alpha. \tag{11}$$

Equation (11) is readily interpreted as the equilibrium conditions of a surface element (Suo & Lu, 2000a).

The system is not in diffusive equilibrium. Consequently, the integral associated with δI_α in Eq. (9) does not vanish. Define the driving force F for diffusion as the free energy reduction associated with one atom moving a unit distance, namely,

$$\int F_\alpha \delta I_\alpha\, dA = -\delta G. \tag{12}$$

This equation requires that the solid be in elastic equilibrium. A comparison of Eqs. (9) and (12) gives

$$F_\alpha = -\frac{\partial}{\Lambda \partial x_\alpha}\left(\frac{\partial g}{\partial C} - 2h_0\nabla^2 C + \phi\varepsilon_{\beta\beta}\right). \qquad (13)$$

This expression gives the driving force at any small element of the monolayer. Observe that the three ingredients – phase separation, phase coarsening, and phase refining – all appear in this expression.

Finally we specify the kinetics, namely, the rate at which the configuration changes. Following Cahn (1961), we assume that the atomic flux is linearly proportional to the driving force,

$$J_\alpha = M F_\alpha. \qquad (14)$$

Here M is the atomic mobility in the monolayer. We have assumed that diffusion is isotropic in the plane of the monolayer. As will become clear, all time scales arc inversely proportional to M.

Evolution equations, scales and parameters

A combination of Eqs. (3), (13) and (14) leads to

$$\frac{\partial C}{\partial t} = \frac{M}{\Lambda^2}\nabla^2\left(\frac{\partial g}{\partial C} - 2h_0\nabla^2 C + \phi\varepsilon_{\beta\beta}\right). \qquad (15)$$

This is a diffusion equation with three kinds of driving forces. It looks similar to that of Cahn (1961) for spinodal decomposition. More will be said about this apparent similarity at the end of this section. Note that the exact thickness of the epilayer does not enter this model. The effect of the layer thickness is contained in the quantity Γ, the excess free energy of the superficial object. Consequently, the model is valid for an epilayer more than a single monolayer, so long as atoms can diffuse within the layer, the layer remains reasonably flat, and the layer thickness is small compared to the in-plane phase size.

In the following numerical simulation, we assume that the epilayer is a regular solution, so that the function $g(C)$ takes the form

$$\begin{aligned} g(C) \;=\; & g_{\mathrm{A}}(1-C) + g_{\mathrm{B}}C + \Lambda kT[C\ln C \\ & + (1-C)\ln(1-C) + \Omega C(1-C)]. \end{aligned} \qquad (16)$$

Here g_{A} and g_{B} are the excess energy of the superficial object when the epilayer is pure A or pure B. (In the special case that A, B and S atoms are all identical, g_{A} and g_{B} reduce to the surface energy of an unstrained one-component solid.) Due to mass conservation, the average concentration is constant when atoms diffuse within the epilayer. Consequently, in Eq. (16) the terms involving g_{A} and g_{B} do not affect diffusion. Only the function in the bracket does. The first two terms in the bracket result from the entropy of mixing, and the third term from the energy of mixing. The dimensionless number Ω measures the exchange energy relative to the thermal energy kT. The $g(C)$ function is convex when $\Omega < 2$, and non-convex when $\Omega > 2$.

Once the surface stress field f is known, Eq. (11) prescribes the surface traction on a half space. The elastic field in the half space due to a tangential point force acting on the surface was solved by Cerruti (see p. 69 in Johnson, 1985). A linear superposition gives the field due to distributed traction on the surface. Only the expression for $\varepsilon_{\beta\beta}$ enters the diffusion driving force. The Cerruti solution gives that

$$\begin{aligned} \varepsilon_{\beta\beta} = & -\frac{(1-\nu^2)\phi}{\pi E} \\ & \times \iint \frac{(x_1-\xi_1)\partial C/\partial\xi_1 + (x_2-\xi_2)\partial C/\partial\xi_2}{[(x_1-\xi_1)^2 + (x_2-\xi_2)^2]^{3/2}}\, d\xi_1\, d\xi_2. \end{aligned} \qquad (17)$$

The integration extends over the entire surface.

A comparison of the first two terms in the parenthesis in Eq. (15) sets a length:

$$b = \left(\frac{h_0}{\Lambda kT}\right)^{1/2}. \qquad (18)$$

This length scales the distance over which the concentration changes from the level of one phase to that of the other. Loosely speaking, one may call b the width of the phase boundary. The magnitude of h_0 is in the order of energy per atom at a phase boundary. Using magnitudes $h_0 \sim 10^{-19}$ J, $\Lambda \sim 5\times 10^{19}\,\mathrm{m}^{-2}$ and $kT \sim 5\times 10^{-21}$ J (corresponding to $T = 400$ K), we estimate that $b = 0.6$ nm.

The competition between coarsening and refining – that is, between the last two terms in Eq. (l5) – sets another length:

$$l = \frac{Eh_0}{(1-\nu^2)\phi^2}. \qquad (19)$$

Young's modulus of a bulk solid is about $E \sim 10^{11}\,\mathrm{N/m^2}$. According to the compilation of Ibach

(1997), the slope of the surface stress is on the order $\phi \sim 4\,\mathrm{N/m}$. These magnitudes, together with $h_0 \sim 10^{-19}\,\mathrm{J}$, give $l \sim 0.6\,\mathrm{nm}$. The numerical simulation shows that the equilibrium phase size is on the order $4\pi l$. This estimate is consistent with the experimentally observed stable phase sizes.

From Eq. (15), disregarding a dimensionless factor, we note that the diffusivity scales as $D \sim MkT/\Lambda$. To resolve events occurring over the length scale of the phase boundary width, b, the time scale is $\tau = b^2/D$, namely,

$$\tau = \frac{h_0}{M(kT)^2}. \tag{20}$$

Equations (15)–(17) define the evolution of the concentration field. Once the concentration field is given at $t = 0$, these equations update the concentration field for the subsequent time. Numerical simulation has been carried out by using a spectrum method (Chen & Shen, 1998; Lu & Suo, 2001). In the simulation, the lengths are given in the unit of b, and the times in τ.

As pointed out above, Eq.(15) looks similar to that of Cahn (1961) for spinodal decomposition. The main difference is how elasticity is introduced. Cahn considered misfit effect caused by composition nonuniformity in the bulk. Such an elasticity effect does *not* refine phases. This is understood as follows. First concentrate on the elasticity effect alone, and disregard the effect of phase boundary energy. Because the theory of elasticity does not have any size scale, the elastic energy is invariant with the phase size, assuming that the phases evolve with self-similar shapes. Once the phase boundary energy is added to the elastic energy, the free energy reduces by phase coarsening. Consequently, no stable pattern is expected. By contrast, the elasticity effect in our model comes from surface stress. This elasticity effect does refine phases.

Simulation results

Figures 8–10 show selected simulation results. In all cases, we have set $b/l = 1$ and $\Omega = 2.2$. For this Ω value, the tangent line in Figure 4 contacts the $g(C)$ curve at $C_\alpha = 0.249$ and $C_\beta = 0.751$. Each calculation cell contains 256×256 grids, with the grid size equal to b. At a given time we plot the levels of the concentration field in the (x_1, x_2) plane in a gray scale.

The four examples shown in Figure 8 are the simulated phase patterns at time $t = 10^5\tau$. For the example in Figure 8a, the average concentration is $C_{\mathrm{ave}} = 0.5$, and the initial concentration field is set to fluctuate randomly within 0.001 from the average. When the simulation starts, the amplitude of the concentration rapidly evolves to the values close to C_α and C_β. The phases organize into a serpentine structure, and stabilize to the size scale shown in Figure 8a at about $t = 10^3\tau$. No significant evolution occurs afterwards. The serpentine structures have been observed experimentally in many systems, including block copolymers (e.g., Park et al., 1997), ferromagnetic films (e.g., Giess, 1980), and the Langmuir monolayers (e.g., Seul & Andelman, 1995). Such systems are typically isotropic in the plane of the films: the stripes do not know which direction to line up. If one views an array of parallel stripes as an analogue of a crystal, the serpentine structure may be viewed as a glass, which adopts the local structure of a crystal, but lacks any long-range order.

The symmetry can be broken in several ways. For the example of Figure 8b, the initial concentration are given some directional preference. Stripes of definite width emerge, and line up in the same direction as prescribed in the initial conditions. The remaining serpentine structure at the edges of the calculation cell will rearrange into straight stripes after some time. The phenomenon is similar to the growth of a crystal at the expense of a glass. This simulation suggests that serpentine structures can transform into an array of stripes if one breaks the symmetry in the initial concentration field at a coarse scale to form 'seeds of the superlattice'. Also present in Figure 8b is a dislocation, which forms when two superlattices grown from different seeds meet. The dislocation will disappear after some time by climbing. In the solid state, the symmetry is broken by various forms of material anisotropy. For example, if the phase boundary energy is anisotropic, straight stripes can also be obtained from a random initial concentration distribution (Lu & Suo, 2001). Presumably the oxide stripes on the (110) Cu surface observed by Kern et al. (l99l) are due to such anisotropy.

For the example of Figure 8c, the average concentration is $C_{\mathrm{ave}} = 0.4$, and the calculation starts from a random initial concentration field. The α phase forms dots, and the β phase forms a continuous matrix. Consistent with Ng and Vanderbilt (1995), our numerical simulation shows that the average concentration affects the type of the phase patterns. The pattern comprises stripes when the average concentration is around 0.5, and dots when the average concentration is somewhat different from 0.5. The phase pattern is also affected by

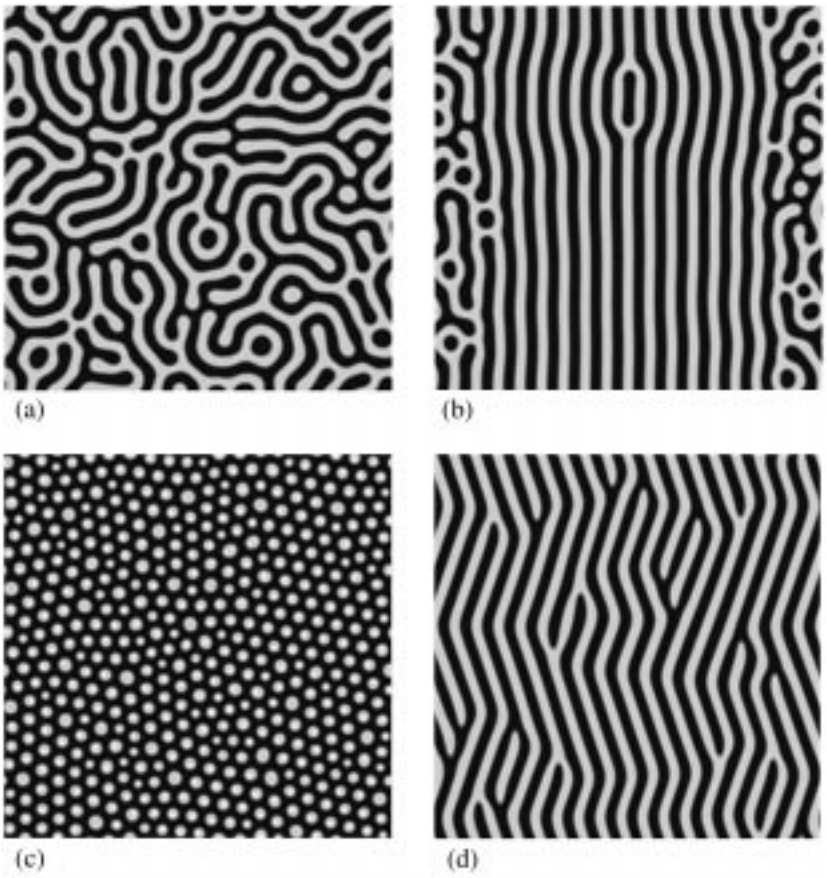

Figure 8. Four simulated phase patterns. Each side of the computation cell is 256*b*. (a) $C_{\text{ave}} = 0.5$ and initial concentration field fluctuates randomly around the average. (b) $C_{\text{ave}} = 0.5$, and the initial concentration field has some directional preference. (c) $C_{\text{ave}} = 0.4$ and initial concentration field fluctuates randomly around the average. (d) $C_{\text{ave}} = 0.5$, initial concentration field fluctuates randomly around the average, and the surface stress is anisotropic.

material anisotropy. For the example in Figure 8c, during the process of evolution, the concentration rapidly attains the values close to C_α and C_β, and the dots settle on the equilibrium size by the time $t \sim 10^3\tau$. Afterwards, the dots try to order into a triangular lattice. The process of spatial ordering is exceedingly slow compared to size selection. Figure 8c shows the typical multi-domain pattern. Dots with local order and polydomains have been observed in many self-assembled two dimensional systems, including block copolymers and the Langmuir films, as well as the recently discovered Lithographically-Induced Self-Assembly (LISA) by Chou and Zhuang (1999). It may be possible to attain long-range order by suitably breaking the symmetry.

In many material systems, the surface stress is anisotropic. Figure 8d shows a phase pattern caused by such anisotropy. The average concentration is $C_{\text{ave}} = 0.5$, and the initial concentration field is random. In the simulation, the coefficient ϕ in the x_2 direction is -0.5 times that in the x_1 direction. The pattern in Figure 8d is reminiscent of the herringbone pattern observed on the (111) Au surface (Narasimhan & Vanderbilt, 1992), although physical details have some dissimilarities.

Figure 9 shows a time sequence of a simulation. The initial condition at $t = 0$ comprises a background concentration 0.4 and six stripes of concentration 0.8. As time goes on, the pattern evolves, but is clearly influenced by the initial conditions. The size of the dots are noticeably nonuniform, but is still of the same scale as that in Figure 8c. Within the time scale shown here, the dots do not order into a triangular lattice. Simulation is stopped at $t = 5000\tau$, although the pattern can

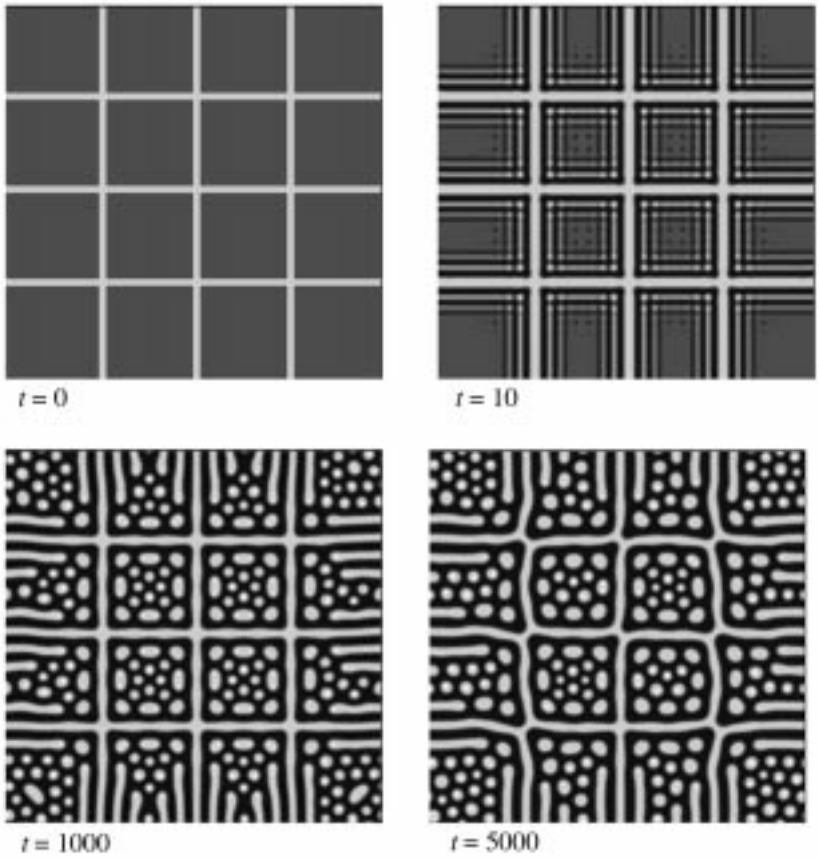

Figure 9. A time sequence initiated with a coarse pattern of concentration field. The subsequent concentration field is affected by both the initial coarse pattern and the self-assembly forces.

still evolve. Figure 10 shows another time sequence, initiated from a different concentration field. Note that at $t = 1000\tau$ a neat pattern has formed in the central region of the computational cell. Both examples show that the pattern at a finite time is influenced by the initial conditions. When a pattern at a coarse scale is introduced, e.g., by the photolithography, the coarse pattern acts like a framework, which influences the self-assembles at a fine scale. Diverse patterns can be produced this way.

Concluding remarks

This paper considers a binary epilayer on a solid surface, where atoms are mobile within the monolayer. The main ingredients for ordering a stable, nanoscopic, periodic phase pattern are identified: (i) unstable solution for phase separation, (ii) phase boundaries for phase coarsening, and (iii) concentration-dependent surface stress for phase refining. We include these ingredients in a phase field model. Numerical simulation shows phases of both stripes and dots, depending on such parameters as the average concentration and material anisotropy. The feature size is of nanoscale, as dictated by the competing actions of the phase boundary energy and the surface stress. During the process of self-assembly, phase separation and size selection take place rapidly. However, long range ordering is very slow, unless suitable anisotropy is introduced. Further simulation is needed to explore possible experimental conditions that will lead to long range ordering.

Acknowledgements

We are grateful to the Department of Energy for the financial support through grant DE-FG02-99ER45787,

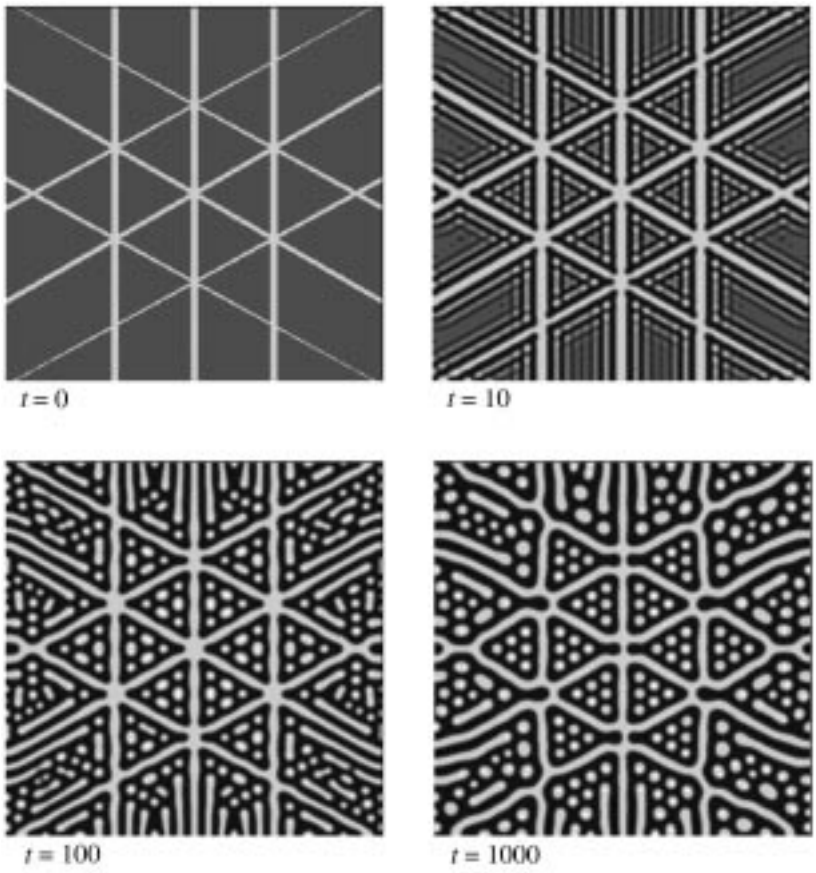

Figure 10. Another time sequence initiated with a different coarse pattern.

and to Dr. M. C. Roco for the invitation to write this article.

References

Ball P., 1999. The Self-Made Tapestry. Oxford University Press, UK.

Böhringer M.K., W.-D. Morgenstern, R. Schneider, F. Berndt, A. Mauri, De Vita & R. Car, 1999. Two dimensional self-assembly of supramolecular clusters and chains. Phys. Rev. Lett. 83, 324–327.

Brune H., M. Giovannin, K. Bromann & K. Kern, 1998. Self-organized growth of nanostructure arrays on strain–relief patterns. Nature 394, 451–453.

Cahn J.W., 1961. On spinodal decomposition. Acta Metall. 9, 795–801.

Cahn J.W. & J.E. Hilliard, 1958. Free energy of a nonuniform system. I. Interfacial free energy. J. Chem. Phys. 28, 258–267.

Cammarata R.C., 1994. Surface and interface stress effects in thin films. Prog. Surf. Sci. 46, 1–38.

Chen L.-Q. & A.G. Khachaturyan, 1993. Dynamics of simultaneous ordering and phase separation and effect of long-range coulomb interactions. Phys. Rev. Lett. 70, 1477–1480.

Chen L.-Q. & J. Shen, 1998. Applications of semi-implicit Fourier-spectral method to phase field equations. Computer Physics Communications 108, 14–158.

Chen L.Q. & Y. Wang, 1996. The continuum field approach to modeling microstructural evolution. JOM 48 (December Issue), 13–18.

Chou S.Y. & L. Zhuang, 1999. Lithographically-induced self-assembly of periodic polymer micropillar arrays. J. Vac. Sci. Tech. B 17, 3197–3202.

Clark P.G. & C.M. Friend, 1999. Interface effects on the growth of cobalt nanostructures on molybdenum-based structures. J. Chem. Phys. 111, 6991–6996.

Giess E.A., 1980. Magnetic-bubble materials. Science 208, 938–943.

Ibach H., 1997. The role of surface stress in reconstruction, epitaxtial growth and stabilization of mesoscopic structures. Surf. Sci. Rep. 29, 193–263.

Johnson K.L., 1985. Contact Mechanics. Cambridge University Press, UK.

Kern K., H. Niebus, A. Schatz, P. Zeppenfeld, J. George & G. Comsa, 1991. Long range spatial self-organization in the adsorbate-induced restructuring of surfaces: Cu{110}−(2×1)O. Phys. Rev. Lett. 67, 855–858.

Lu W. & Z. Suo, 1999. Coarsening, refining, and pattern emergence in binary epilayers. Zeitschrift fur Metallkunde, 90, 956–960.

Lu W. & Z. Suo, 2001. Dynamics of nanoscale pattern formation of an epitaxtial monolayer. Prepared for a special issue of Journal of the Mechanics and Physics of Solids dedicated to Professors of J.W. Hutchinson and J.R. Rice on the occasion of their 60th birthdays.

Martin J.W., R.D. Doherty & B. Cantor, 1997. Stability of Microstructure in Metallic Systems. 2nd edn. Cambridge University Press, UK.

Murray C.B., C.R. Kagan & M.G. Bawendi, 2000. Synthesis and characterization of monodisperse nanocrystals and close-packed nanocrystal assemblies. Annu. Rev. Mater. Sci. 30, 545–610.

Narasimhan S. & D. Vanderbilt, 1992. Elastic stress domain and herringbone reconstruction on Au (111). Phys. Rev. Lett. 69, 1564–1567.

Ng K.-O. & D. Vanderbilt, 1995. Stability of periodic domain structures in a two dimensional dipolar model. Phys. Rev. B 52, 2177–2183.

Park M., C. Harrison, P.M. Chaikin, R.A. Register & D.H. Adamson, 1997. Block copolymer lithography: periodic arrays of $\sim 10^{11}$ holes in 1 square centimeter. Science 276, 1401–1404.

Parker T.M., L.K. Wilson & N.G. Condon, 1997. Epitaxy controlled by self-assembled nanometer-scale structures. Phys. Rev. B 56, 6458–6461.

Pohl K., M.C. Bartelt, J. de la Figuera, N.C. Bartelt, J. Hrbek & R.Q. Hwang, 1999. Identifying the forces responsible for self-organization of nanostructures at crystal surfaces. Nature 397, 238–241.

Röder H., R. Schuster, H. Brune & K. Kern, 1993. Monolayer-confined mixing at the Ag–Pt(111) interface. Phys. Rev. Lett. 71, 2086–2089.

Seul M. & D. Andelman. Domain shapes and patterns: the phenomenology of modulated phases. Science 267, 476–483.

Su C.H. & P.W. Voorhees, 1996. The dynamics of precipitate evolution in elastically stressed solids. Acta Mater 44, 1987–2016.

Suo Z., 2000. Evolving materials structures of small feature sizes. Int. J. Solids Structures. 37, 367–378.

Suo Z. & W. Lu, 2000a. Composition modulation and nanophase separation in a binary epilayer. J. Mech. Phys. Solids. 48, 211–232.

Suo Z. & W. Lu, 2000b. Self-organizing nanophases on a solid surface. In: Chuang T.J., ed. Multi-Scale Deformation and Fracture in Materials and Structures. A book dedicated to Professor James R. Rice on the occasion of his 60th birthday. (to be published by Kluwer Academic Publishers)

Timoshenko S.P. & J.N. Goodier, 1970. Theory of Elasticity. McGraw-Hill Book Company, New York.

Vanderbilt D., 1997. Ordering at surfaces from elastic and electrostatic interactions. Surface Rev. Lett. 4, 811–816.